Open Archive Toulouse Archive Ouverte (OATAO)

To cite this version:

Spin crossover in Fe(triazole)−Pt nanoparticle self-assembly structured at the sub-5 nm scale†

Suhail Usmani,[a] Mirko Mikolasek, [ID][b,c] Angélique Gillet,[a] José Sanchez Costa, [ID][b,d] Mathilde Rigoulet,[a] Bruno Chaudret, [ID][a] Azzedine Bousseksou,[b] Benedikt Lassalle Kaiser,[e] Phillipe Demont,[f] Gábor Molnár, [ID][b] Lionel Salmon, [ID][b] Julian Carrey[a] and Simon Tricard [ID] *[a]

A main goal of molecular electronics is to relate the performance of devices to the structure and electronic state of molecules. Among the variety of possibilities that organic, organometallic and coordination chemistries offer to tune the energy levels of molecular components, spin crossover phenomenon is a perfect candidate for elaboration of molecular switches. The reorganization of the electronic state population of the molecules associated to the spin crossover can indeed lead to a significant change in conductivity. However, molecular spin crossover is very sensitive to the environment and can disappear once the molecules are integrated into devices. Here, we show that the association of ultra-small 1.2 nm platinum nanoparticles with Fe^{II} triazole-based spin crossover coordination polymers leads to self-assemblies, extremely well organized at the sub-3 nm scale. The quasi-perfect alignment of nanoparticles observed by transmission electron microscopy, in addition to specific signature in infrared spectroscopy, demonstrates the coordination of the long-chain molecules with the nanoparticles. Spin crossover is confirmed in such assemblies by X-ray absorption spectroscopic measurements and shows unambiguous characteristics both in magnetic and charge transport measurements. Coordinating polymers are therefore ideal candidates for the elaboration of robust, well-organized, hybrid self-assemblies with metallic nanoparticles, while maintaining sensitive functional properties, such as spin crossover.

[a] Laboratoire de Physique et Chimie des Nano Objets, INSA, CNRS, Université de Toulouse, Toulouse, France. E mail: tricard@insa toulouse.fr

[b] Laboratoire de Chimie de Coordination, CNRS, Université de Toulouse, Toulouse, France

[c] ESRF The European Synchrotron, Grenoble, France

[d] IMDEA Nanociencia, Ciudad Universitaria de Cantoblanco, Madrid, Spain

[e] Synchrotron SOLEIL, L'Orme des Merisier, Gif sur Yvette, France

[f] Institut Carnot Centre Inter universitaire de Recherche et d'Ingénierie des Matériaux, INP ENSIACET, CNRS, Université de Toulouse, Toulouse, France

Introduction

Arrays of nanoparticles (NPs) have been extensively studied associated with individual molecules. Among them NPs have been used as nanoelectrodes to connect molecules.[1–5] In such systems, electrons jump from one NP to another. The limiting elements of the current flow are molecules and equivalent circuits are generally assimilated to resistors and capacitors in series. Several reports focused on molecular effects in nanoparticle arrays, as the length of the molecule,[6,7] its redox state,[8] its charge,[9] its conjugation,[10] etc. Recently, we demonstrated that using ultra-small NPs (<2 nm), it was possible to observe Coulomb blockade regime at room temperature in metal NP arrays.[11] This finding was particularly interesting as the same transport regime could be observed on a large range of temperature. Charge transport was then determined by the polarizability of the molecules, as demonstrated with simple thiol functionalized alkyl chains or aromatic cycles.[11]

Spin crossover (SCO) molecular compounds show reversible switching between the low spin and high spin states of the central metal ion. The SCO thus corresponds to a reorganization of the electron density of the metal center, which can be modulated by different external parameters: temperature, pressure, light irradiation, electric field, etc.[12–14] This electronic state population reorganization leads to the modification of the charge transport through the molecule,[15–18] which has been evidenced at different scales: on microcrystals,[19] nanoparticles,[20] thin layers,[21] and molecules dispersed in a matrix.[22] Several attempts have also been reported towards measurements on the single molecule scale,[23] mostly using scanning tunneling microscopy.[24,25] Synthesizing hybrid systems combining metallic NPs and SCO molecules is an interesting alternative towards this ultimate size scale, as NPs act as local electrodes at the nanoscale and SCO molecules show at least two electronic states that influence the charge transport between the NPs in the network. A recent study reported the synthesis of core–shell NPs formed by a 12 nm Au

core surrounded by a 4 nm shell of an insulating SCO coordination polymer. Electrical measurements on aggregates of such objects showed a significantly higher conductivity than the corresponding coordination network and a higher current switching ratio between the two spin states.[26] In another attempt, SCO molecules were combined with arrays of gold NPs and the charge transport behavior was correlated with the magnetic properties of the coordination complexes.[27]

Generally, authors choose thiols to attach functional molecules to metallic (e.g. Au, Pt, Ag) NPs, in order to stabilize the hybrid systems thanks to the strong interaction between the generated thiolates and the metal surface.[28–30] However, the sulfur-metal bond is very energetic and might be too strong to favor the binding-unbinding process, necessary to obtain well-organized molecule-nanoparticle self-assemblies (SA) at large scale. In addition, one can doubt that this strong bond does not affect the SCO in the molecule because of the electronic and steric constraint it imposes. To avoid such drawbacks we chose building blocks in order to obtain stable and robust assemblies: (1) Fe(triazole) based coordination polymer, where three triazole ligands bridge two Fe^{II} centers, geometry which thus increases the stability of the molecular system; (2) ultra-small PtNPs (1.2 ± 0.3 nm), which limit the increase of electronic density in proximity to the Fe^{II} centers; (3) coordination of the molecular polymer to the NP surface by thiophene moieties, which bind Pt less strongly than thiols and thus allows more flexibility and adaptability during the SA process.[31] By this strategy, we obtained a hybrid system, consisting of lamellae where the NPs aligned with a periodicity of 3 nm. Specific lamellar SA of nanoparticles have already been reported, with liquid crystals,[32] diblock copolymers,[33–35] or peptidic polymers.[36] But to our knowledge, even if demonstrated for molecular clusters,[37] no work has described organization of ultra-small NPs in quasi perfect linear assemblies with a periodicity lower than 5 nm, so far.

Results and discussion

Synthesis of the hybrid system

The PtNPs were synthesized by decomposition of $Pt_2(dba)_3$ (dba = dibenzylideneacetone) under a carbon monoxide (CO) atmosphere in THF, followed by washing of the organic dba ligands with pentane, as previously reported.[11,38] Transmission electron microscopy (TEM) pictures showed well dispersed NPs, with diameters of 1.2 nm ± 0.3 nm (Fig. 1a). Such NPs are particularly interesting as, in addition to their ultra-small sizes, they can be seen as "naked", i.e. free of organic ligand, as they are only stabilized by CO from the synthesis and THF, a coordinating solvent.[39] The other building block of the SA was a triazole based Fe^{II} coordination polymer (Fig. 1b). Such polymers are well referenced in the literature: they are robust, show SCO at temperatures close to room temperature and can easily be processed in nanoparticles, thin films, hybrid materials with polymers, and so forth.[40–46] An advantage of the triazole moiety is its possibility of functionalization, which has already been extensively used to tune the
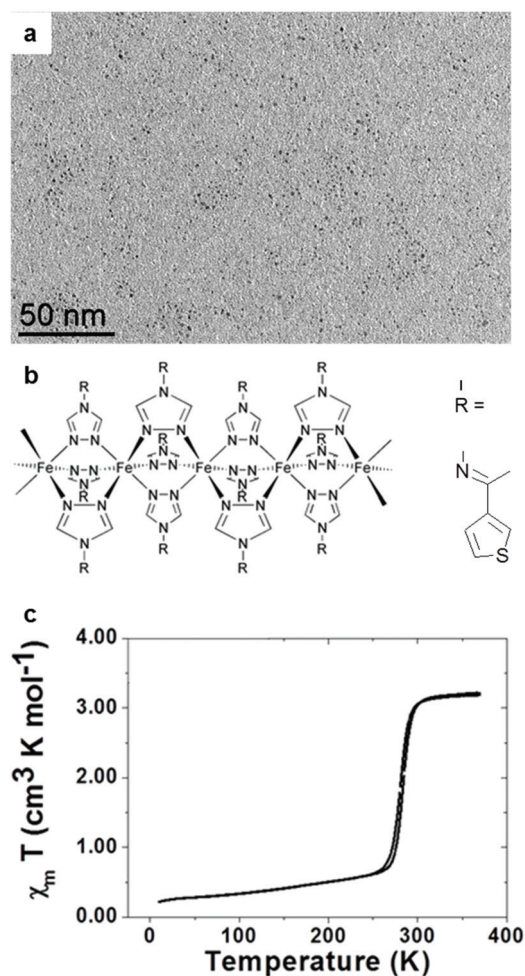
Fig. 1 Building blocks. (a) TEM image of pristine ultra small (1.2 ± 0.3 nm) platinum nanoparticles. (b) Schematic illustration of the FeL_3 coordination polymer   L = (1E) 1 (thiophen 3 yl) N (4H 1,2,4 triazol 4 yl)ethan 1 imine. Fe triazole networks form unidimensional structures, where two Fe^{II} centers are linked to each other by three bridging triazole ligands. (c) Magnetic measurement on the FeL_3 coordination polymer in the 'gel state', showing an abrupt SCO at 285 K. The curve is normalized per mole of Fe.

SCO,[40] and sometimes to control shaping of objects at the nanoscale.[19,47] Here, we chose a thiophene functionalization, which coordinate to the Pt surface thanks to the strong affinity between S and Pt, but not too strongly to facilitate its relative dissociation, necessary to the SA trial-and-error process.[48,49] We thus synthesized the L ligand (L = (1E)-1-(thiophen-3-yl)-N-(4H-1,2,4-triazol-4-yl)ethan-1-imine) by the condensation of 4-aminotriazole with acetylthiophene. Mixing three equivalent of L with one equivalent of $Fe(oTs)_2 \cdot 6H_2O$ (oTs = tosylate) in THF led to the formation of the $FeL_3(oTs)_2$ coordination polymer, called FeL_3. We first checked that this new compound showed SCO close to room temperature. We indeed confirm that the $\chi_M T$ product (where χ_M is the molar magnetic susceptibility) sharply increased with temperature at 285 K (Fig. 1c). It is important to note that this magnetic behavior corresponds to a light-yellow gel sample with partially evapor-

ated THF solvent (*sic* 'gel state'), whereas the pale-white, fully dry powder (*sic* 'powder state') remains in the high spin state at any temperature (see ESI Fig. S1†).

Description of the self-assembly

SA between the NPs and the SCO compound was carried out in the same solvent: solutions of NPs, **L** and Fe(oTs)$_2$·6H$_2$O were mixed together and agitated in THF for two hours. The obtained hybrid SA is called PtNPs-Fe**L**$_3$ SA. The precursor concentrations were adapted to obtain 0.2 equivalents (eq.) of **L** and 0.06 eq. of Fe per introduced Pt. The equivalent number (eq.) is defined as the ratio between the quantity of ligands or Fe and the quantity of platinum atoms present in the system. These ratios were chosen to keep the Fe : **L** ratio equal to 1 : 3 (as in the coordination polymer), and to have a **L** : Pt ratio equal to 0.2 : 1, as it was previously demonstrated to be the equivalence ratio, when all the ligands are coordinated at the NP surface.[11] TEM images of the PtNPs-Fe**L**$_3$ SA showed zones were the ultra-small PtNPs were perfectly aligned (Fig. 2a and ESI Fig. S2a, b, c†), forming parallel lines separated by 3.2 nm from each other. A basic geometrical model suggests that a single strand of polymer separates the NP lines (Fig. 2b). We verified that such a structuration was not induced by the presence of **L** alone: without Fe(oTs)$_2$ but only **L**, the NPs aggregated, probably thanks to the bridging aspect of the ligand with triazole on one side and thiophene on the other one, but no alignment was observed (ESI Fig. S2d†).

Fourier-transform infra-red (FT-IR) spectroscopy was performed on the pristine PtNPs, after addition of **L** only, and on the SA after addition of **L** and the iron salt (Fig. 2c and d). The spectrum of the pristine NPs showed an intense peak at 2043 cm^{-1} corresponding to the vibration of terminal CO, and two smaller peaks at 1805 and 1880 cm^{-1} corresponding to two modes of vibration of bridging CO. Following the vibration position of terminal CO by FT-IR spectroscopy is an efficient tool to probe the electronic density at the NP surface. The significant shift of the vibration from 2043 to 2033 cm^{-1} is compatible with the coordination of **L** at the PtNP surface, which turns to be richer in electron. Indeed, higher electronic density at the surface implies stronger back-donation from the NP to the antibonding orbitals of the CO molecule, and a thus vibration at a lower wavenumber.[50] The coordination of the iron salts to the other side of the **L** ligand in the hybrid SA takes electronic density back, and leads to a CO vibration back to 2042 cm^{-1}. Such a behavior in FT-IR is in good agreement with the coordination of **L** at the PtNP surface and the electronic withdrawing effect of the Fe centers linked to the PtNP by coordination through **L**. This work thus shows for the first
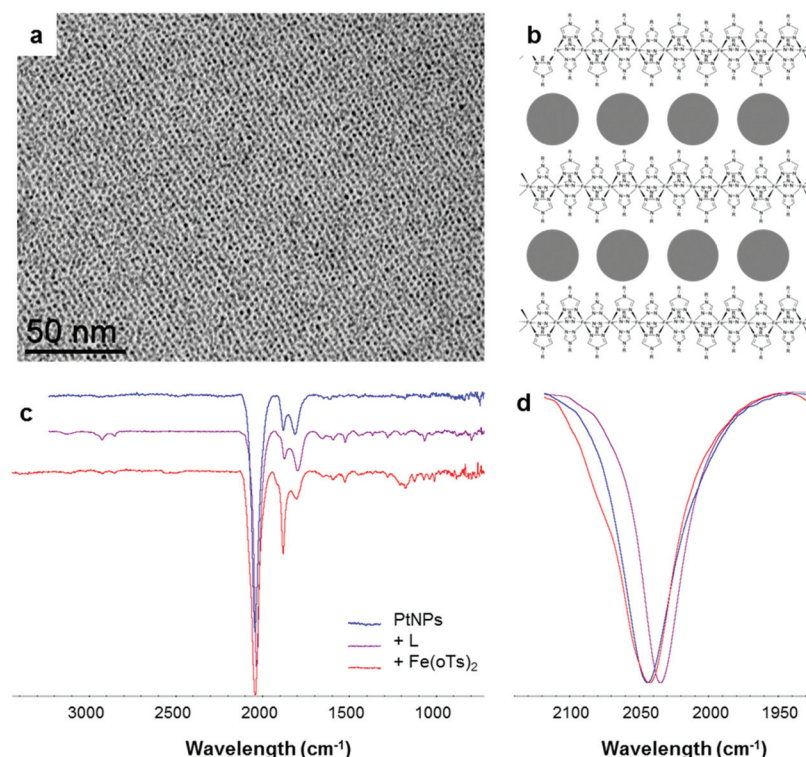
Fig. 2 Hybrid self assembly made of Pt nanoparticles (NPs) and Fe**L**$_3$ coordination polymers. (a) TEM image of the self assembly. (b) Structural model of the self assembly, showing the intercalation of coordination polymers and aligned NPs. Infrared spectra of the pristine PtNPs, after addition of **L**, and after addition of **L** and the iron salt Fe(oTs)$_2$·6H$_2$O: (c) full spectra (the baselines are shifted for clarity) and (d) zoom on the terminal CO region. The shift of the CO bond vibration from 2043 to 2033 cm^{-1} is a signature of the **L** coordination at the PtNP surface, which turns to be richer in electron; the coordination of the iron salts to the other side of the **L** ligand takes electronic density back, and leads to a shift of the CO bond vibration back to 2042 cm^{-1}.
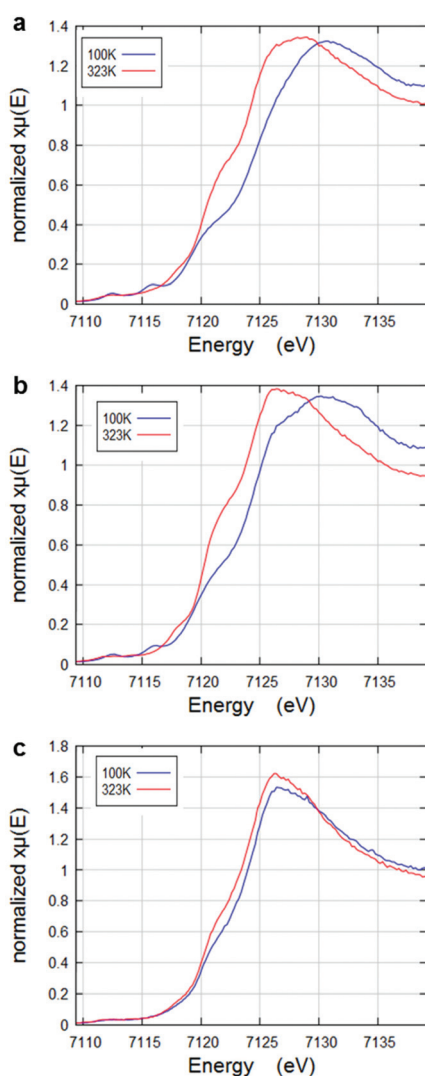
time that an appropriate coordination between coordination polymers and metal NPs can lead to well-organized hybrid system, at a sub-5 nm scale.

Spin crossover in the hybrid system

Spectroscopic characterizations are irrefutable proofs of the presence of SCO in a system as complex as our SAs. We thus performed X-Ray near edge absorption spectroscopy (XANES) measurements at the Fe K-edge, as the iron atom is the SCO center. As an element of comparison, we first measured spectra of $[Fe(NH_2Trz)_3]Br_2$ (NH_2Trz = 2-amino-1,2,4-triazole), known to show a full SCO between 260 and 310 K.[51] We observed a shift of the Fe K-edge energy towards lower values between 100 K (low spin) and 323 K (high spin), attributed to the SCO signature (Fig. 3a). A similar shift was observed in the
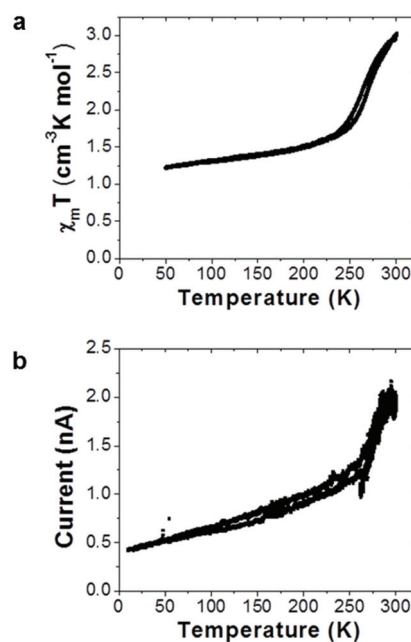
FeL_3 coordination polymer and, in a smaller proportion, in the PtNPs-FeL_3 SA (Fig. 3b and c). In order to estimate the proportion of Fe that underwent SCO in each samples, we compared the shifts between the two curves in low and high spin states to the one of the $[Fe(NH_2Trz)_3]Br_2$ reference, for which we considered a full SCO.[52,53] SCO was thus estimated to be equal to 89% in the FeL_3 coordination polymer alone, and to 36% in the PtNPs-FeL_3 SA. XAS measurements thus proved that SCO was present, to some extent, in the self-assembled system. In magnetic measurements on the FeL_3 coordination polymer, $\chi_M T$ value decreased from 3.2 to 0.4 cm^{-3} K mol^{-1} while decreasing the temperature from 320 K to 100 K (Fig. 1c), a difference that corresponds to a decrease of 88% of the magnetization, in very good agreement with the spin population conversion of 89% estimated by XANES measurements between these two temperatures.

Magnetic and charge transport measurements

Magnetic measurement on PtNPs-FeL_3 SA showed an incomplete, abrupt and slightly hysteretic transition in the 'gel state' (Fig. 4a). In this sample, the $\chi_M T$ value decreased from 3.0 to 1.7 cm^{-3} K mol^{-1} while decreasing the temperature from 300 K to 250 K. This decrease of 42% of magnetization is in the same order of magnitude as the 36% of SCO determined by XAS. This incomplete and relatively gradual SCO in the PtNPs-FeL_3 SA could arise from three different sources. The first possible reason is intrinsic and can be due to the presence of the platinum NPs, which might block SCO, as they

Fig. 3 Spin crossover. XAS measurements at 100 K and 323 K at the Fe K edge on (a) $[Fe(NH_2Trz)_3]Br_2$ (NH_2Trz = 4 amino 1,2,4 triazole). (b) FeL_3 coordination polymer. (c) PtNPs FeL_3 self assembly. By comparison with the $[Fe(NH_2Trz)_3]Br_2$ reference, known to show a full spin crossover at 310 K, the spin crossover was estimated to be equal to 89% in the FeL_3 coordination polymer, and to 36% in the PtNPs FeL_3 self assembly.

Fig. 4 Magnetic and electrical measurements on the PtNPs FeL_3 self assembly. (a) Magnetic measurement. The curve is normalized per mole of Fe. (b) Electrical measurement. The slope break around 280 K in the current characteristics can be attributed to the spin crossover observed in magnetic measurements and demonstrated by XAS measurements (Fig. 3).

bring high electronic density in the vicinity of the Fe[II] center. A second reason can come from the inhomogeneity of the SA: some parts of it, well-organized, would switch, whereas the other ones would not. The third reason is more experimental and could come from a quantity of remaining solvent not sufficiently high. Indeed, as for the coordination polymer, no SCO was observed anymore on PtNPs-Fe**L**₃ SA in the dry 'powder state', where the system remained at the high spin state (ESI Fig. S3†).

Transport measurements were performed on SA deposited on interdigitated electrodes by drop casting. During the measurements, the temperature was swept at the rate of 1 K min⁻¹. Below 250 K, the current slope decreased gradually towards low temperatures (Fig. 4b). Decrease in current at low temperature is a typical characteristic of arrays of NPs separated by molecules and can arise due to the less thermal energy available to overcome the charging energy.[54–57] However, this description does not explain the sharp decrease (increase) in current during cooling (heating) cycle observed between 250 K and 300 K. Charge transport in hybrid compounds with ultra-small nanoparticles is governed by Coulomb blockade, even at room temperature,[11] as observed in the PtNPs-Fe**L**₃ SA (ESI Fig. S4†). Coulomb blockade is directly linked to the polarizability of the compounds surrounding the nanoparticles,[11] *i.e.* the coordination polymer here. During the SCO from the low to the high spin state, the antibonding orbitals of the iron center are populated, increasing the Fe–N bound distance and thus the polarizability of the coordination compound. As a result, the dielectric constant is (in general) higher in the high spin state, as already demonstrated.[58] As a direct consequence, the conductivity of the high spin state is higher than that of the low spin state in the hybrid system.

Resistance of the hybrid assemblies varied in the range of $10–10^3$ MΩ for different assemblies, and voltages ranging between few tenths of a volt up to 2 V (ESI Fig. S5†). The current values were observed in the range of few nA to few hundred nA. In other experiments, a cycle opening was observed in the current–temperature curve when the temperature was swept at 3 K min⁻¹ (ESI Fig. S6†). Faster sweeping rate thus results in a temperature lag, which gives rise to a hysteresis-like curve in the current–temperature cycles.

Magnetic measurement and charge transport measurements on the PtNPs-Fe**L**₃ SA show similar behaviors. While the $\chi_M T$ rapidly decreases from 300 K to 250 K in magnetic measurements, current also shows a relatively sharp decrease in roughly the same temperature regime. Such changes in conductivity can arise due to several factors. Different charge transport mechanism such as sequential tunneling and co-tunneling could result in changes in current–temperature slope.[57] However, we unlikely believe this hypothesis because such a transport mechanism change typically takes place at lower temperatures. In our case, we have observed a sharp change in the current near 250 K. So far, the most likely explanation of the observed transport behavior comes from the SCO process where the current follows the same behavior as the magnetic moment in magnetic measurements. The high spin state is then the more conducting state, as already observed in hybrid systems made of metal NPs and NCO coordination molecules.[20,27]

Conclusion

In summary, we have shown that mixtures of a coordination polymer with ultra-small platinum nanoparticles can afford well-organized SA, where lines of NPs intercalated with single polymer strands. The key aspect of this SA is the coordination of the polymer to the NP surface by the thiophene moiety, sufficiently strong to ensure the system cohesion, but not too strong to facilitate the elements' rearrangement. Such an approach is particularly interesting to build hybrid material structures at the lower than 5 nm scale, for which thermal energy is too high to assemble the building blocks by van der Waals forces only.[59] Besides, the robustness of the triazole based coordination polymer gave the opportunity to maintain its SCO functional properties, even in the hybrid SA, as confirmed by XAS measurements. The consequence of such a SCO implied significant discrepancies in the magnetic and electrical characteristics of the sample.

In the future, to ensure optimal performances, the rational design of hybrid SA including metallic NPs and functional molecules, should consider ultra-small NPs, robust molecular systems such as coordination polymers and a fine tuning of the chemical interaction between the anchoring moiety of the functional molecules and the NP surface, as demonstrated in this work.

Experimental methods

Chemical syntheses

Ligand L. 4-Amino-4*H*-1,2,4 triazole (2 g, 0.023 M) and 3-acetylthiophene (2.9 g, 0.023 M) were mixed in 50 mL ethanol and the solution was stirred and heated overnight at reflux. The solution was partially evaporated and a white solid was obtained (yield 80%). ¹H NMR (400 MHz, DMSO, δ, ppm): 2.35 (3H, s), 7.66 (1H, d), 7.73 (1H, d), 8.43 (1H, s), 8.78 (2H, s). Elemental analysis (%): Calc. C: 50.00; H: 4.20; N: 29.10. Obs. C: 49.76; H: 4.05; N, 29.34.

FeL₃ **coordination polymer.** 10 mL of a solution of the **L** ligand (at 6×10^{-3} mol L⁻¹ in THF) and 10 mL of a solution of Fe(oTs)₂·6H₂0 (at 2×10^{-3} mol L⁻¹ in THF–oTs = paratoluene sulfonate) were mixed under vigorous stirring. The precursor concentrations were adapted to obtain 3 equivalent of the **L** ligand per Fe. The solution was agitated for 2 hours. The remaining solution was partially evaporated to a light yellow-gel called 'gel state'. Evaporation was stopped when an equivalent of 50% in mass of solvent remained in the system. A particular care to avoid evaporation has to be taken for characterization as the THF is particularly volatile. Further evaporation to dryness led to a pale white powder called 'powder state'. TEM images of the pristine Fe**L**₃ coordination polymer do not show any presence of nanostructure objects.

Platinum nanoparticles. The PtNPs have been synthesized as previously described.[11,38] All operations were carried out using Fischer–Porter bottle techniques under argon. A solution of $Pt_2(dba)_3$ (90 mg; 0.165 mmol of Pt) in 20 mL of freshly distilled and deoxygenated THF was pressurized in a Fischer–Porter bottle with 1 bar of CO during 30 minutes at room temperature under vigorous stirring. During this time, the solution color changed from violet to brown (attesting the formation of the NPs). The mixture was evaporated and washed with pentane to eliminate the dba (3×20 mL), and to obtain native NPs. The colloid was then redissolved in 20 mL of THF. The size of the NPs was found to be equal to 1.2 ± 0.3 nm. For each series of measurements, the sizes were determined by TEM imaging.

Self-assembly. 1 mL of a solution of the **L** ligand (at 6×10^{-3} mol L^{-1} in THF) and 1 mL of a solution of $Fe(oTs)_2 \cdot 6H_2O$ (at 2×10^{-3} mol L^{-1} in THF) were simultaneously added to 4 mL of the native NP mixture under vigorous mixing. The precursor concentrations were adapted to obtain 0.2 eq. of **L** and 0.06 eq. of Fe per introduced Pt. The brown solution was agitated for 2 hours. Drops of the crude solution were deposited on specific substrates for each characterization (see below). The remaining solution was partially evaporated to a viscous liquid called 'gel state'. Evaporation was stopped when an equivalent of 50% in mass of solvent remained in the system. A particular care to avoid evaporation has to be taken for characterization as the THF is particularly volatile. Further evaporation to dryness led to a dark-brown powder called 'powder state'. The self-assembly experiments have been repeated several times and led to reproducible results. The systems presented here come from optimization of the experimental conditions, in the scope of a larger study where different parameters have been tested (varying the equivalent numbers, the nature of the counter-ions, the order of addition of the building blocks, *etc.*).

Structural characterization of the assemblies

Samples for TEM were prepared by deposition of one drop of the crude solution on a carbon covered holey copper grid. TEM analyses were performed at the "centre de microcaractérisation Raimond Castaing" using a JEOL JEM 1400 electron microscope operating at 120 kV. The mean size of the particles was determined by image analysis on a large number of particles (~300) using the ImageJ software. Scanning transmission electron microscopy with energy dispersive X-ray spectroscopy (STEM-HAADF/EDS) analysis was performed on a JEOL JEM-ARM200F Cold FEG operated at 200 kV.

FT-IR spectra were recorded on a Thermo Scientific Nicolet 6700 FT-IR spectrometer in the range 4000–700 cm^{-1}, using a Smart Orbit ATR platform. The sample deposition was performed by drop casting of the crude solution on the germanium crystal of the platform; the measurement was acquired after evaporation of the THF solvent.

XAS measurements

X-ray absorption spectra were collected on the LUCIA beamline of SOLEIL at a ring energy of 2.75 GeV and a ring current of 500 mA. The energy was monochromatized thanks to a Si(311) double crystal monochromator and the data were collected as fluorescence excitation spectra using a silicon drift detector (Bruker). The energy of the beamline was calibrated to the first inflection point of a metallic iron foil (7112.0 eV). All data were normalized using the Athena software of the IFEFFIT package. The reference sample $[Fe(NH_2Trz)_3]Br_2$ was measured as a diluted powder in a graphite pellet. To maintain the PtNPs-Fe**L**$_3$ and PtNPs-Fe**L**$_3$ samples in a 'gel state' and avoid THF evaporation during measurement, we used a home-made liquid sample holder where the gel was placed and sealed with a Kapton window. The difference of shifts of the Fe K absorption edge between the low and high spin curves was determined to quantify SCO. Even if some differences can be observed between HS and LS states in the pre-edge structure, differences are significantly higher comparing the absorption edges.[60,61] Comparison of such shift were calculated by determining the area delimited by the two curves in the low and high spin states, between $x\mu(E)$ values equal to 0.4 and 1. We then calculated the ratios between the areas of interest and the one of the reference $[Fe(NH_2Trz)_3]Br_2$ compound, in which a 100% SCO was assumed. SCO was thus estimated to be equal to 89% in the Fe**L**$_3$ coordination polymer alone, and to 36% in the PtNPs-Fe**L**$_3$ SA. The estimation of SCO can vary from ±10%; that is why we integrated the area of interest on a range of $x\mu(E)$ values as large as possible.

Magnetic measurements

PPMS-VSM from Quantm design was used to perform the magnetic measurements during which the magnetic moment from the sample was measured at a constant magnetic field of 1.5 T while varying the temperature at 1 K min^{-1}. The sample was carefully placed in a closed cylindrical sample holder of known mass which is placed in VSM such that it experiences the field in the direction perpendicular to its cross-section. For sample in the gel state, temperature was never set above 300 K, in order to avoid solvent evaporation. Evaluation of susceptibility from magnetic moment requires the mass of the measured sample inside the sample holder. This was calculated by weighing the measured sample and subtracting the mass of empty sample holder from it. For the samples measured in gel state, an additional mass of the solvent present in the sample could result in inaccurate values of susceptibility. In order to avoid this, the sample was left to dry after the measurement until there was no reduction in mass due to solvent evaporation. The mass of the dried sample was then carefully recorded for further calculation of susceptibility. The pristine PtNPs did not give any magnetic signal as they are diamagnetic.

Charge transport measurements

The electrodes for transport measurements consisted of eight pairs of interdigitated combs elaborated by photolithography.[62,63] They were composed of 20 interpenetrated fingers with a height of 30 nm, a length of 200 μm, and separated by a gap of 5 μm. Integration of the particles

between the electrodes was performed by dropcasting of 10 μL of solution on the electrode. To do so, a droplet of the colloidal solution was deposited on the sample. After twenty seconds, the droplet was dried using an absorbing paper. Transport measurements were performed in a nitrogen-cooled cryostat using a Keithley 6430 subfemtoamperemeter. The slope break attributed to spin crossover was observed in four out of the six measured electrodes.

Conflicts of interest

There are no conflicts to declare.

Acknowledgements

References

1 A. Zabet-Khosousi and A.-A. Dhirani, *Chem. Rev.*, 2008, **108**, 4072–4124.

2 M. Pauly, J.-F. Dayen, D. Golubev, J.-B. Beaufrand, B. P. Pichon, B. Doudin and S. Bégin-Colin, *Small*, 2012, **8**, 108–115.

3 Y. Zhou, S.-T. Han, Z.-X. Xu and V. A. L. Roy, *Adv. Mater.*, 2012, **24**, 1247–1251.

4 A. Nag, D. S. Chung, D. S. Dolzhnikov, N. M. Dimitrijevic, S. Chattopadhyay, T. Shibata and D. V. Talapin, *J. Am. Chem. Soc.*, 2012, **134**, 13604–13615.

5 J. Liao, S. Blok, S. J. van der Molen, S. Diefenbach, A. W. Holleitner, C. Schönenberger, A. Vladyka and M. Calame, *Chem. Soc. Rev.*, 2015, **44**, 999–1014.

6 D. Conklin, S. Nanayakkara, T.-H. Park, M. F. Lagadec, J. T. Stecher, M. J. Therien and D. A. Bonnell, *Nano Lett.*, 2012, **12**, 2414–2419.

7 J. Dugay, R. P. Tan, M. Ibrahim, C. Garcia, J. Carrey, L.-M. Lacroix, P.-F. Fazzini, G. Viau and M. Respaud, *Phys. Rev. B: Condens. Matter Mater. Phys.*, 2014, **89**, 041406.

8 J. Liao, J. S. Agustsson, S. Wu, C. Schönenberger, M. Calame, Y. Leroux, M. Mayor, O. Jeannin, Y.-F. Ran, S.-X. Liu and S. Decurtins, *Nano Lett.*, 2010, **10**, 759–764.

9 H. Moreira, J. Grisolia, N. M. Sangeetha, N. Decorde, C. Farcau, B. Viallet, K. Chen, G. Viau and L. Ressier, *Nanotechnology*, 2013, **24**, 095701.

10 S. J. van der Molen, J. Liao, T. Kudernac, J. S. Agustsson, L. Bernard, M. Calame, B. J. van Wees, B. L. Feringa and C. Schönenberger, *Nano Lett.*, 2009, **9**, 76–80.

11 S. Tricard, O. Said-Aizpuru, D. Bouzouita, S. Usmani, A. Gillet, M. Tassé, R. Poteau, G. Viau, P. Demont, J. Carrey and B. Chaudret, *Mater. Horiz.*, 2017, **4**, 487–492.

12 *Spin Crossover in Transition Metal Compounds I*, ed. P. Gütlich and H. A. Goodwin, Springer-Verlag, Berlin Heidelberg, 2004.

13 A. Bousseksou, G. Molnár, L. Salmon and W. Nicolazzi, *Chem. Soc. Rev.*, 2011, **40**, 3313.

14 M. A. Halcrow, *Spin–Crossover Materials: Properties and Applications*, Wiley-Blackwell, Chichester, West Sussex, United Kingdom, 2013.

15 C. Lefter, V. Davesne, L. Salmon, G. Molnár, P. Demont, A. Rotaru and A. Bousseksou, *Magnetochemistry*, 2016, **2**, 18.

16 E. Ruiz, *Phys. Chem. Chem. Phys.*, 2014, **16**, 14–22.

17 G. Molnár, S. Rat, L. Salmon, W. Nicolazzi and A. Bousseksou, *Adv. Mater.*, 2018, **30**, 1703862.

18 A. Bellec, J. Lagoute and V. Repain, *C. R. Chim.*, 2018, **21**, 1287–1299.

19 A. Rotaru, I. A. Gural'skiy, G. Molnár, L. Salmon, P. Demont and A. Bousseksou, *Chem. Commun.*, 2012, **48**, 4163–4165.

20 F. Prins, M. Monrabal-Capilla, E. A. Osorio, E. Coronado and H. S. J. van der Zant, *Adv. Mater.*, 2011, **23**, 1545–1549.

21 T. Mahfoud, G. Molnár, S. Cobo, L. Salmon, C. Thibault, C. Vieu, P. Demont and A. Bousseksou, *Appl. Phys. Lett.*, 2011, **99**, 053307.

22 M. Matsuda, H. Isozaki and H. Tajima, *Chem. Lett.*, 2008, **37**, 374–375.

23 E. A. Osorio, K. Moth-Poulsen, H. S. J. van der Zant, J. Paaske, P. Hedegård, K. Flensberg, J. Bendix and T. Bjørnholm, *Nano Lett.*, 2010, **10**, 105–110.

24 T. G. Gopakumar, F. Matino, H. Naggert, A. Bannwarth, F. Tuczek and R. Berndt, *Angew. Chem., Int. Ed.*, 2012, **51**, 6262–6266.

25 T. Miyamachi, M. Gruber, V. Davesne, M. Bowen, S. Boukari, L. Joly, F. Scheurer, G. Rogez, T. K. Yamada, P. Ohresser, E. Beaurepaire and W. Wulfhekel, *Nat. Commun.*, 2012, **3**, 938.

26 R. Torres-Cavanillas, R. Sanchis-Gual, J. Dugay, M. Coronado-Puchau, M. Giménez-Marqués and E. Coronado, *Adv. Mater.*, 2019, **31**, 1900039.

27 E. J. Devid, P. N. Martinho, M. V. Kamalakar, I. Šalitroš, Ú. Prendergast, J.-F. Dayen, V. Meded, T. Lemma, R. González-Prieto, F. Evers, T. E. Keyes, M. Ruben, B. Doudin and S. J. van der Molen, *ACS Nano*, 2015, **9**, 4496–4507.

28 D. V. Talapin, J.-S. Lee, M. V. Kovalenko and E. V. Shevchenko, *Chem. Rev.*, 2010, **110**, 389–458.

29 A. Courty, J. Richardi, P.-A. Albouy and M.-P. Pileni, *Chem. Mater.*, 2011, **23**, 4186–4192.

30 J. P. Coelho, G. González-Rubio, A. Delices, J. O. Barcina, C. Salgado, D. Ávila, O. Peña-Rodríguez, G. Tardajos and A. Guerrero-Martínez, *Angew. Chem., Int. Ed.*, 2014, **53**, 12751–12755.

31 T. B. Rauchfuss, in *Progress in Inorganic Chemistry*, ed. S. J. Lippard, John Wiley & Sons, Inc., Hoboken, NJ, USA, 2007, pp. 259–329.

32 M. Mitov, C. Portet, C. Bourgerette, E. Snoeck and M. Verelst, *Nat. Mater.*, 2002, **1**, 229–231.

33 Y. Lin, A. Böker, J. He, K. Sill, H. Xiang, C. Abetz, X. Li, J. Wang, T. Emrick, S. Long, Q. Wang, A. Balazs and T. P. Russell, *Nature*, 2005, **434**, 55–59.

34 Y. Zhao, K. Thorkelsson, A. J. Mastroianni, T. Schilling, J. M. Luther, B. J. Rancatore, K. Matsunaga, H. Jinnai, Y. Wu, D. Poulsen, J. M. J. Fréchet, A. P. Alivisatos and T. Xu, *Nat. Mater.*, 2009, **8**, 979–985.

35 V. B. Leffler, L. Mayr, P. Paciok, H. Du, R. E. Dunin-Borkowski, M. Dulle and S. Förster, *Angew. Chem., Int. Ed.*, 2019, **58**, 8541–8545.

36 G. Manai, *et al.*, *Submitted*.

37 Z. Wu, J. Liu, Y. Gao, H. Liu, T. Li, H. Zou, Z. Wang, K. Zhang, Y. Wang, H. Zhang and B. Yang, *J. Am. Chem. Soc.*, 2015, **137**, 12906–12913.

38 S. Gomez, L. Erades, K. Philippot, B. Chaudret, V. Collière, O. Balmes and J.-O. Bovin, *Chem. Commun.*, 2001, 1474–1475.

39 F. Dassenoy, K. Philippot, T. Ould Ely, C. Amiens, P. Lecante, E. Snoeck, A. Mosset, M.-J. Casanove and B. Chaudret, *New J. Chem.*, 1998, **22**, 703–712.

40 O. Roubeau, *Chem. – Eur. J.*, 2012, **18**, 15230–15244.

41 Y.-S. Koo and J. R. Galán-Mascarós, *Adv. Mater.*, 2014, **26**, 6785–6789.

42 D. Qiu, D.-H. Ren, L. Gu, X.-L. Sun, T.-T. Qu, Z.-G. Gu and Z. Li, *RSC Adv.*, 2014, **4**, 31323–31327.

43 A. Holovchenko, J. Dugay, M. Giménez-Marqués, R. Torres-Cavanillas, E. Coronado and H. S. J. van der Zant, *Adv. Mater.*, 2016, **28**, 7228–7233.

44 L. Moulet, N. Daro, S. Mornet, N. Vilar-Vidal, G. Chastanet and P. Guionneau, *Chem. Commun.*, 2016, **52**, 13213–13216.

45 Z.-H. Li, Y.-X. Wang, W.-K. Han, W. Zhu, T. Li, Z. Li, X. Ren and Z.-G. Gu, *New J. Chem.*, 2017, **41**, 10062–10068.

46 L. Salmon and L. Catala, *C. R. Chim.*, 2018, **21**, 1230–1269.

47 H. Peng, G. Molnár, L. Salmon and A. Bousseksou, *Eur. J. Inorg. Chem.*, 2015, **2015**, 3336–3342.

48 M. Karimi, H. R. L. Z. Zhad, F. Aboufazeli, O. Sadeghi and E. Najafi, *J. Inorg. Organomet. Polym. Mater.*, 2013, **23**, 385–392.

49 M. Gadogbe, S. M. Ansar, I.-W. Chu, S. Zou and D. Zhang, *Langmuir*, 2014, **30**, 11520–11527.

50 C. Dablemont, P. Lang, C. Mangeney, J.-Y. Piquemal, V. Petkov, F. Herbst and G. Viau, *Langmuir*, 2008, **24**, 5832–5841.

51 O. Kahn, J. Kröber and C. Jay, *Adv. Mater.*, 1992, **4**, 718–728.

52 V. Briois, Ph. Sainctavit, G. J. Long and F. Grandjean, *Inorg. Chem.*, 2001, **40**, 912–918.

53 M.-L. Boillot, J. Zarembowitch, J.-P. Itié, A. Polian, E. Bourdet and J. G. Haasnoot, *New J. Chem.*, 2002, **26**, 313–322.

54 R. Parthasarathy, X.-M. Lin and H. M. Jaeger, *Phys. Rev. Lett.*, 2001, **87**, 186807.

55 J. Liao, M. A. Mangold, S. Grunder, M. Mayor, C. Schönenberger and M. Calame, *New J. Phys.*, 2008, **10**, 065019.

56 H. Moreira, Q. Yu, B. Nadal, B. Bresson, M. Rosticher, N. Lequeux, A. Zimmers and H. Aubin, *Phys. Rev. Lett.*, 2011, **107**, 176803.

57 J.-F. Dayen, E. Devid, M. V. Kamalakar, D. Golubev, C. Guédon, V. Faramarzi, B. Doudin and S. J. van der Molen, *Adv. Mater.*, 2013, **25**, 400–404.

58 A. Bousseksou, G. Molnár, P. Demont and J. Menegotto, *J. Mater. Chem.*, 2003, **13**, 2069–2071.

59 B. Abécassis, F. Testard and O. Spalla, *Phys. Rev. Lett.*, 2008, **100**, 115504.

60 V. Briois, C. Cartier dit Moulin, P. Sainctavit, C. Brouder and A.-M. Flank, *J. Am. Chem. Soc.*, 1995, **117**, 1019–1026.

61 G. Vankó, T. Neisius, G. Molnár, F. Renz, S. Kárpáti, A. Shukla and F. M. F. de Groot, *J. Phys. Chem. B*, 2006, **110**, 11647–11653.

62 J. Dugay, R. P. Tan, A. Meffre, T. Blon, L.-M. Lacroix, J. Carrey, P. F. Fazzini, S. Lachaize, B. Chaudret and M. Respaud, *Nano Lett.*, 2011, **11**, 5128–5134.

63 A. Rotaru, J. Dugay, R. P. Tan, I. A. Guralskiy, L. Salmon, P. Demont, J. Carrey, G. Molnár, M. Respaud and A. Bousseksou, *Adv. Mater.*, 2013, **25**, 1745–1749.

Supporting information

Spin crossover in Fe(triazole)-Pt nanoparticle self-assembly structured at the sub-5 nm scale

Suhail Usmani,[a] Mirko Mikolasek,[b,c] Angélique Gillet,[a] José Sanchez Costa,[b,d] Mathilde Rigoulet,[a]

Bruno Chaudret,[a] Azzedine Bousseksou,[b] Benedikt Lassalle-Kaiser,[e] Phillipe Demont,[f] Gábor

Molnár,[b] Lionel Salmon,[b] Julian Carrey,[a] and Simon Tricard[a,*]

[a] *Laboratoire de Physique et Chimie des Nano-Objets, INSA, CNRS, Université de Toulouse,*

Toulouse, France

[b] *Laboratoire de Chimie de Coordination, CNRS, Université de Toulouse, Toulouse, France*

[c] *ESRF-The European Synchrotron, Grenoble, France*

[d] *IMDEA Nanociencia, Ciudad Universitaria de Cantoblanco, Madrid, Spain*

[e] *Synchrotron SOLEIL, L'Orme des Merisier, Gif-sur-Yvette, France*

[f] *Institut Carnot – Centre Inter-universitaire de Recherche et d'Ingénierie des Matériaux, INP-*

*ENSIACET, CNRS, Université de Toulouse, Toulouse, France*

[*] *Corresponding author: tricard@insa-toulouse.fr*

Content: statement of contributions, supplementary experimental data.

Statement of contributions: All authors participated to the planning, discussed the results and contributed to the preparation of the manuscript. JSC and LS synthesized and characterized the ligand and the complex. ST, AG and MR worked on the Pt nanoparticle synthesis, self-assembly and characterization. ST, SU, AG, MM and BLK carried out XAS measurements. SU and JC carried out or analyzed magnetic and transport measurements.
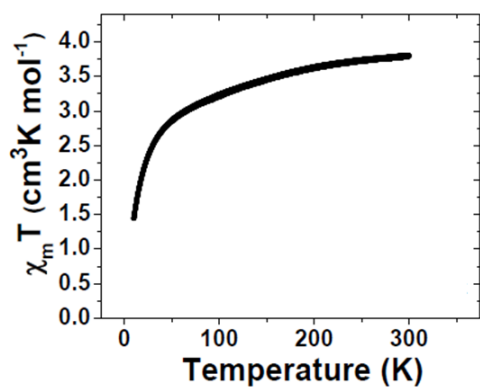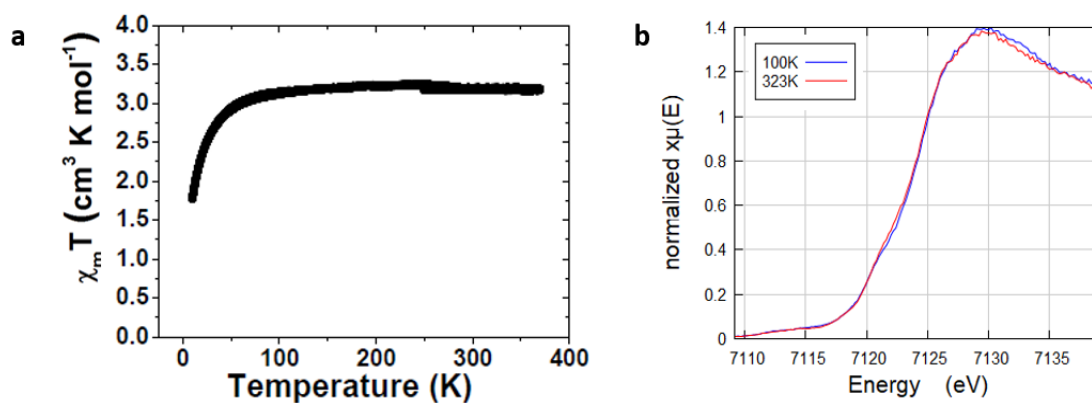
Fig. S1 Loss of spin crossover in the 'powder state'. Magnetic measurement on the Fe**L**$_3$ coordination polymer in the dry 'powder state'. The curve is normalized per mole of Fe. The decrease of $\chi_m T$ at low temperature is attributed to zero-field splitting.
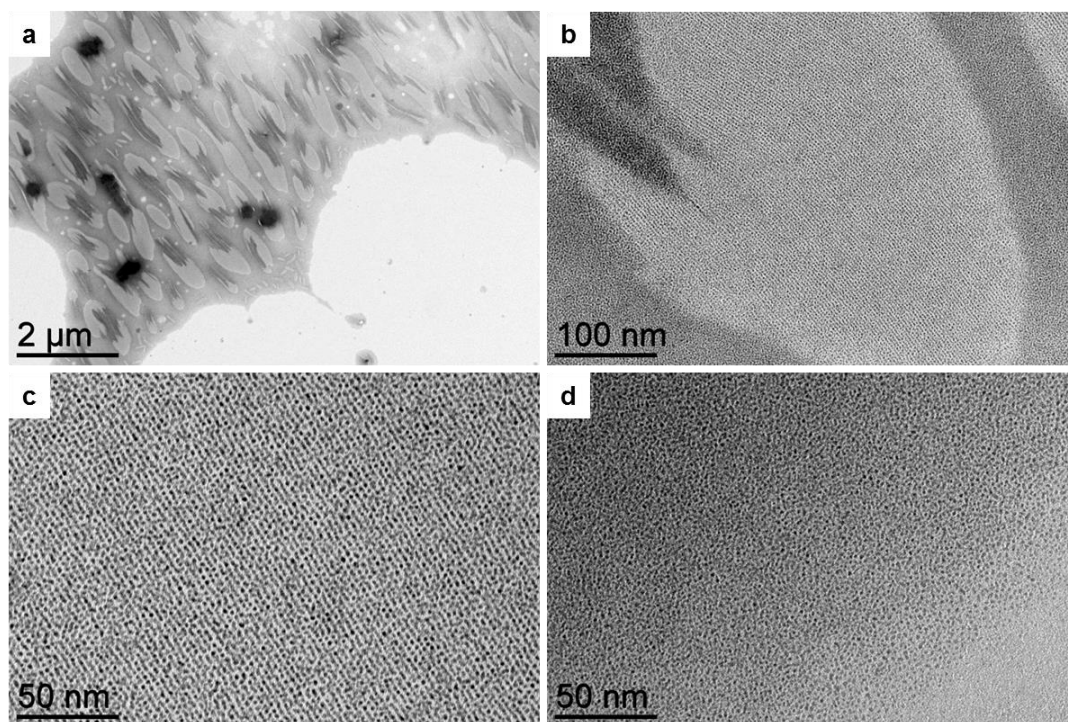
Fig. S2 Hybrid self-assembly made of Pt nanoparticles (NPs) and FeL$_3$ coordination polymers. (a, b, c) TEM images of the self-assembly at different magnifications (Fig. S2c is identical to Fig. 2a). The hybrid system is constituted by zones of NP lines distributed in larger areas where the PtNPs are disorganized. (d) TEM image after mixing of PtNPs with **L** only. No NP line is observed in absence of Fe(oTs)$_2$.

Fig. S3 Loss of spin crossover of the PtNPs-FeL_3 self-assembly in the 'powder state': (a) Magnetic measurement. The curve is normalized per mole of Fe. The sample stays high spin at all temperatures; the decrease of $\chi_m T$ at low temperature is attributed to zero-field splitting. (b) XAS measurement. The curves are identical at low and high temperature.
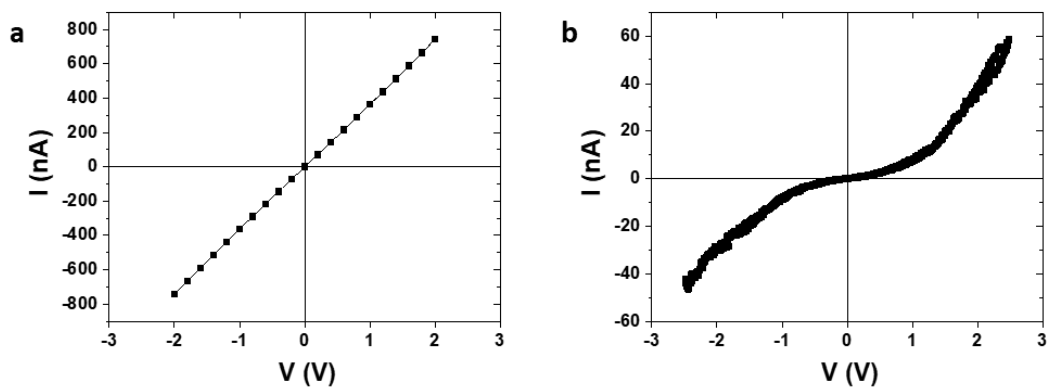
Fig. S4 I-V characteristics at 300K: (a) on a deposit of the pristine PtNPs; (b) on the PtNPs-Fe**L**$_3$ self-assembly. The non-linearity of the curve for the self-assembly is the signature of the presence of Coulomb blockade (see *e.g.* S. Tricard, O. Said-Aizpuru, D. Bouzouita, S. Usmani, A. Gillet, M. Tassé, R. Poteau, G. Viau, P. Demont, J. Carrey and B. Chaudret, *Mater Horiz*, 2017, **4**, 487–492).
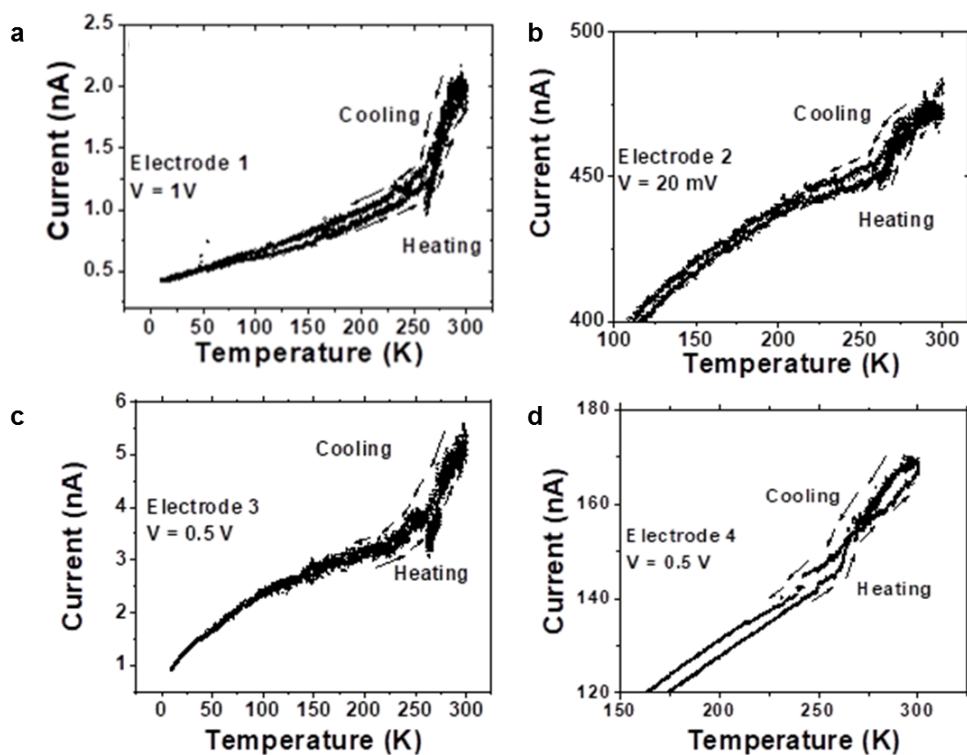
Fig. S5 Electrical measurements on the PtNPs-Fe**L**$_3$ self-assembly on independent electrodes, biased at different voltages: (a) 1V; (b) 20 mV; (c) 0.5V; (d) 0.5 V, with sweeping rate of 1K.min^{-1}. All the curves slope breaks around 270 K can be attributed to the spin crossover. The significant difference in resistance between the electrodes is attributed to non-homogeneous filling of the interdigitated electrodes by the materials.
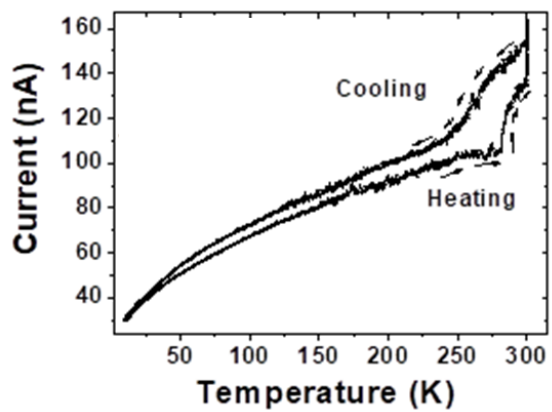
Fig. S6 Hysteresis opening in electrical measurements on the PtNPs-Fe**L**$_3$ self-assembly, on electrodes biased at voltage of 0.1V, with a sweeping rate of 3 K.min^{-1}.